

3D VDE Benchmark

C. R. Sovinec,¹ S. C. Jardin,² F. J. Artola,³ and I. Krebs⁴

¹*University of Wisconsin-Madison*

²*Princeton Plasma Physics Laboratory*

³*ITER Organization*

⁴*Dutch Institute for Fundamental Energy Research*

acknowledgments to

Matthias Hölzl, Cesar Clauser, and Nate Ferraro

Center for Tokamak Transient Simulation Meeting

May 13, 2020



*Center for Tokamak
Transient Simulation*

Outline

- Introduction (Carl)
 - Motivation
 - NSTX case
 - Summary of 2D benchmarking
- 3D problem setup
 - NIMROD-specific information and results (Carl)
 - M3D-C1-specific information and results (Steve)
- Comparisons (Steve)
- Conclusions (Steve)

Our motivation is to verify codes and models that can be used for VDE studies.

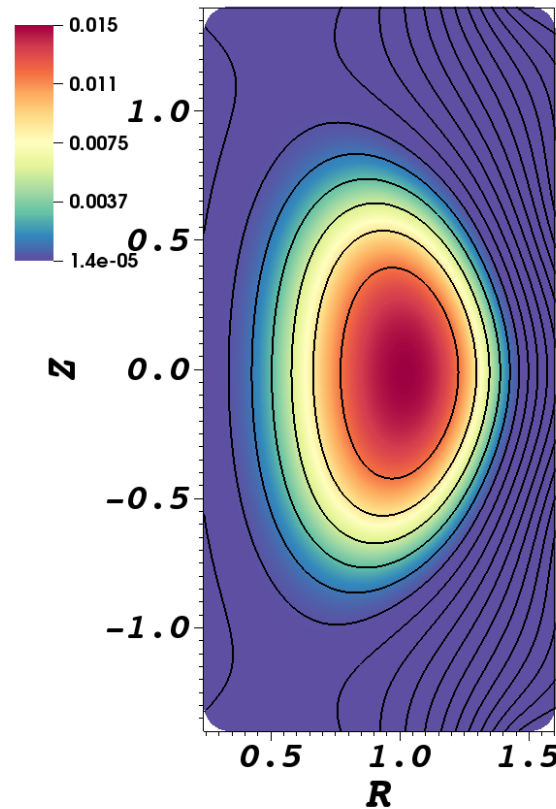
- NIMROD, M3D-C1, and JOREK are being applied to 2D and 3D disruption studies.
- Each has been verified with analytical results and with code comparisons on other applications.
- The comparisons reported here provide verification information on a realistic nonlinear VDE application.
- The 3D benchmarking is the FES theory milestone for this fiscal year's third quarter.

The three codes differ in their models and in their numerical methods.

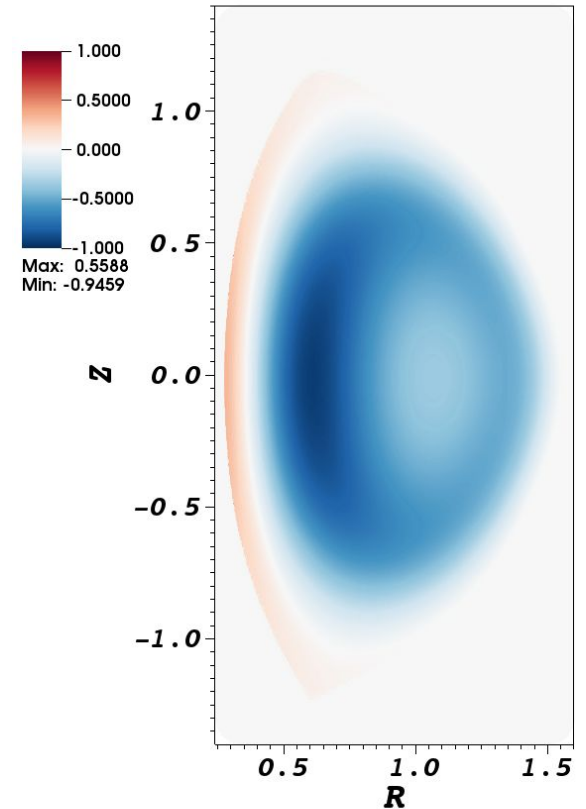
	NIMROD	M3D-C1	JOEK
MHD model	full	full	reduced used here
Resistive wall/ vacuum	thin/meshed used here	thick/ meshed	thin/Green's
Linear/ nonlinear	both	both	both
Poloidal representation	nodal spectral elements	reduced quintics	Bezier cubics
Toroidal rep.	Fourier	Hermite cubics	Fourier
Temporal advance	semi-impl./ implicit	implicit	implicit

This benchmark is based on an NSTX discharge that allowed vertical instability.

- Discharge #139536 had feedback partially turned off during the shot.
- David Pfefferlé conducted a simulation-based study of this case, previously. [PoP **25**, 056105 (2018)]
- Benchmark computations use a simplified wall shape.
- The initial state is from 309 ms and is VDE-unstable.



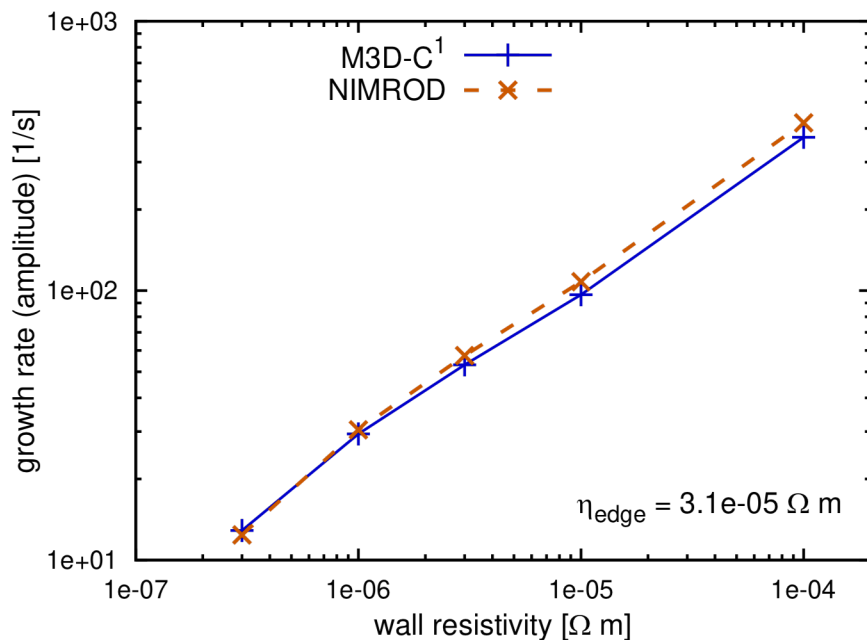
Equilibrium $\mu_0 P$ and Ψ .



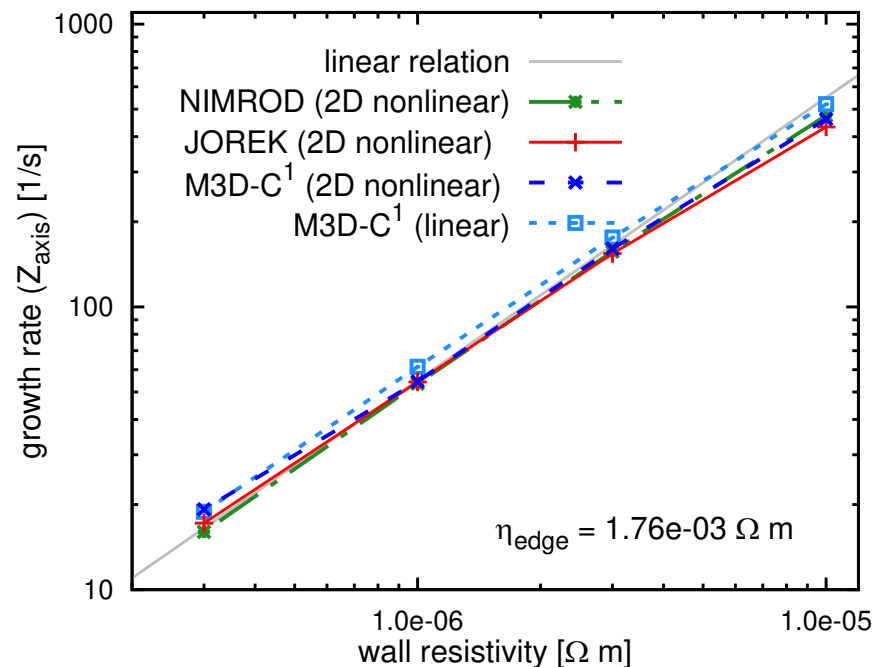
Equilibrium $\mu_0 J_\phi / R$.

The 2D benchmarking considered linear and nonlinear evolution.¹

- VDE growth rates from linear computations and from the linear phase of 2D nonlinear computations agree among the codes to within 15%.



Growth-rates from linear computations are within 4% at the smallest η_{wall} and within 13% at the largest η_{wall} .

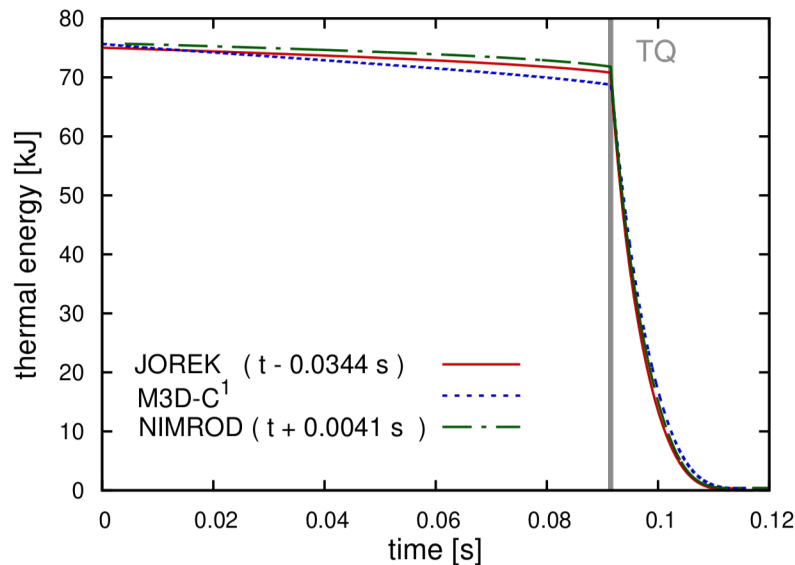


Growth rates from nonlinear computations were based on fitting $Z_{\text{axis}}(t) = a + be^{-\gamma t}$.

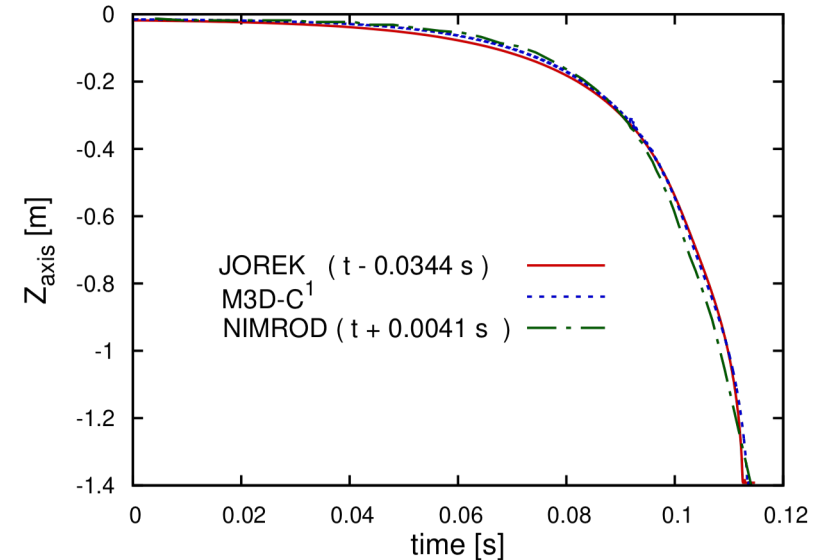
¹I. Krebs, *et al.*, Phys. Plasmas **27**, 022505 (2020).

Nonlinear 2D computations were run though plasma termination.

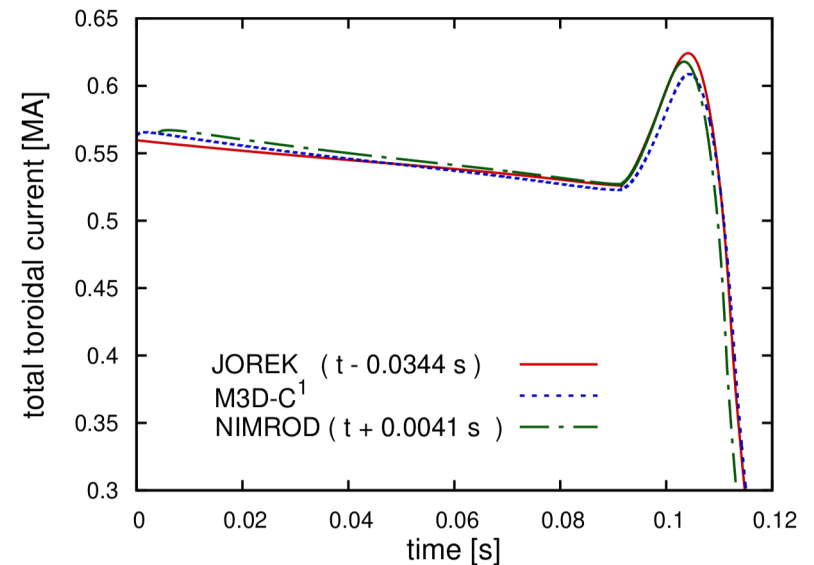
- The κ_{\perp} and D values were increased by 500 and 20, respectively, when the LCFS contacted the wall.
- Besides the benchmarking, the study shows that reduced-MHD does well with $RB_{\phi} \cong (RB_{\phi})_{vac}$, even at low R/a .



The fast thermal quench results from the increase in thermal conduction.



Evolution of vertical position of magnetic axis.



Plasma current spikes when conduction broadens the current-density distribution.

Computations for the 3D comparison have larger diffusion coefficients.

Coefficient	Publ. 2D case pre LCFS contact	Publ. 2D case post LCFS contact	New 2D pre LCFS contact	3D post LCFS contact
η_0 (Ohm-m)	3.12×10^{-5}	3.12×10^{-5}	3.12×10^{-4}	3.12×10^{-4}
η_w (Ohm-m)	3×10^{-6}	3×10^{-6}	3×10^{-5}	3×10^{-5}
D (m ² /s)	0.154	3.08	1.54	40.
κ_{\perp} (1/m·s)	1.54×10^{18}	7.70×10^{20}	1.54×10^{19}	1.54×10^{21}
κ_{\parallel} (1/m·s)	1.54×10^{23}	1.54×10^{23}	1.54×10^{24}	1.54×10^{26}
ν (kg/m·s)	5.16×10^{-7}	5.16×10^{-7}	5.16×10^{-7}	5.16×10^{-7}

- The plasma resistivity is $\eta(T) = \eta_0(T_0/T)^{3/2}$, $T_0 = 15$ eV.
- $\tau_A \cong 1 \mu\text{s}$.
- The change in thermal conductivity at LCFS contact starts the thermal quench in 2D and 3D computations.

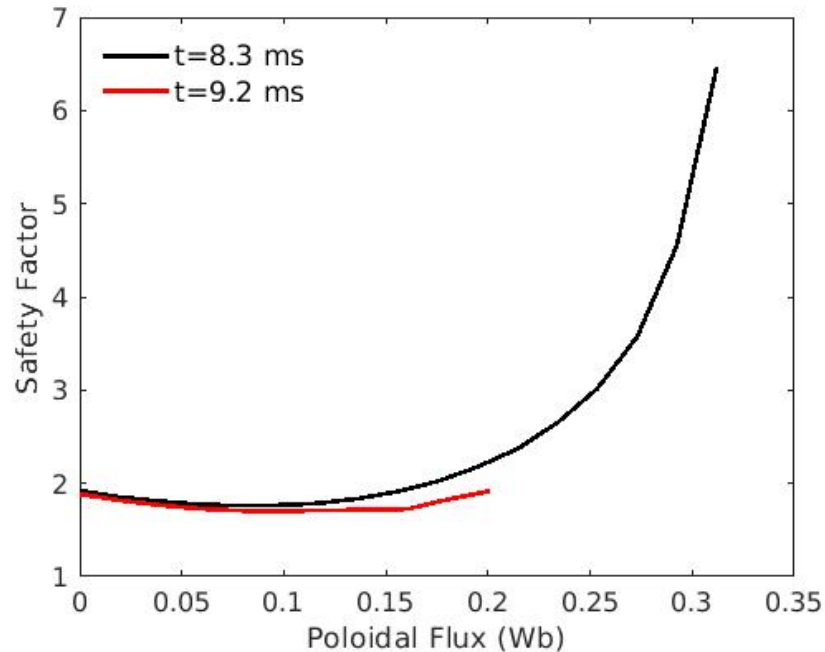
NIMROD-specific information includes spatial resolution, time-stepping, and force computation.

- Poloidal meshing has $\sim 39,000$ bicubic elements in the plasma region.
- 3D computations have $0 \leq n \leq 10$ or $0 \leq n \leq 21$.
- For accuracy with NIMROD's implicit leapfrog, the flow-CFL number is not allowed to exceed unity.
- Net force on the resistive wall is computed as a surface integral.
 - $F_j = \mu_0^{-1} \oint d\mathbf{S} \cdot \left[\mathbf{B}\mathbf{B} - \underline{\underline{\mathbf{I}}} B^2 / 2 \right] \cdot \hat{\mathbf{e}}_j$
 - Integrating over the outer surface, only, is sufficient given that plasma inertia is small.¹
- At 9.4 ms (1.1 ms into 3D phase), $v_{||} = 100v$ is introduced to avoid mesh-scale noise on the tokamak's outboard side.

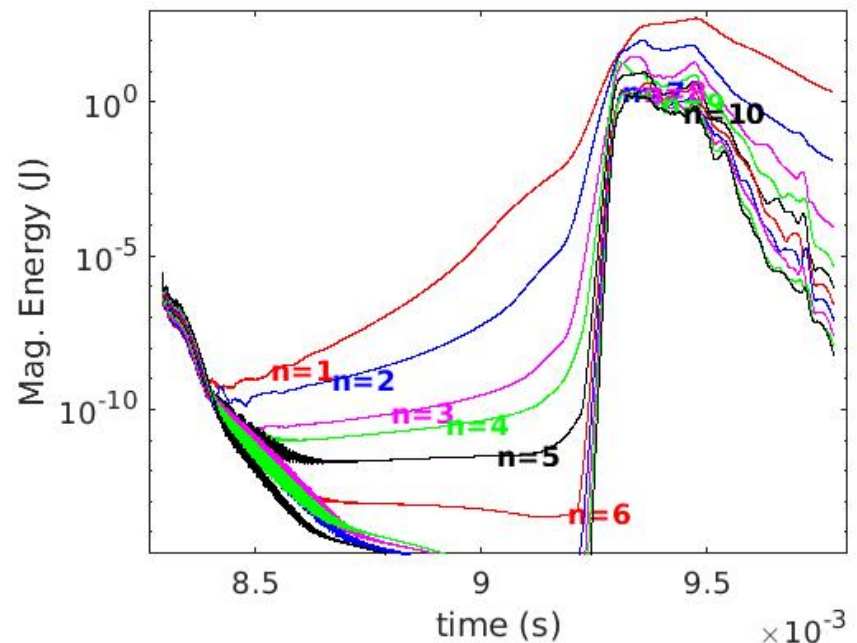
¹V. D. Pustovitov, Nucl. Fusion **55**, 113032 (2015).

The 3D computations evolve for nearly 1 ms before significant activity arises.

- Edge flux surfaces are removed through wall contact.
- The $n=1$ modes remain small until the edge q -value decreases to 2.

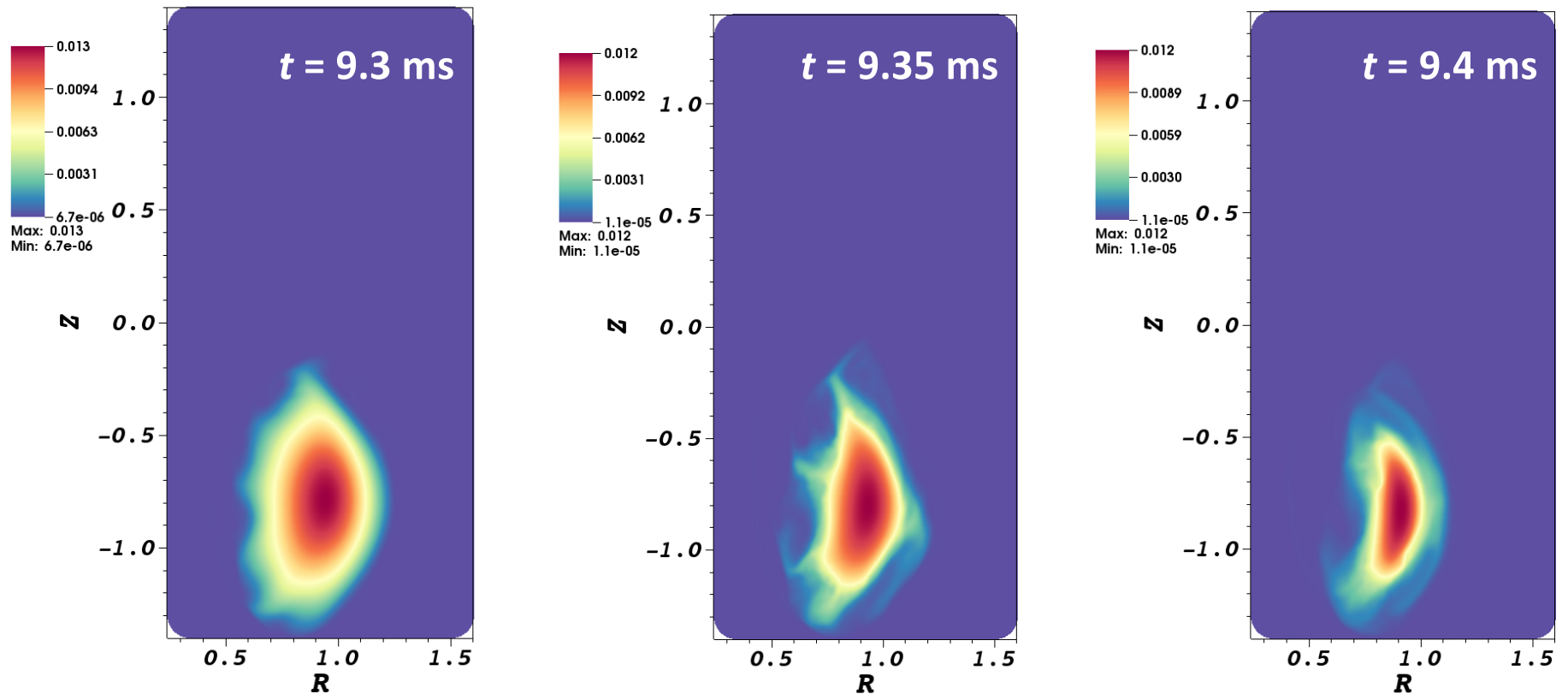


Approximate q -profiles at the beginning of the 3D computation and when growth rates increase.



Magnetic fluctuation energy evolution shows significant activity starting at 9.2 ms.

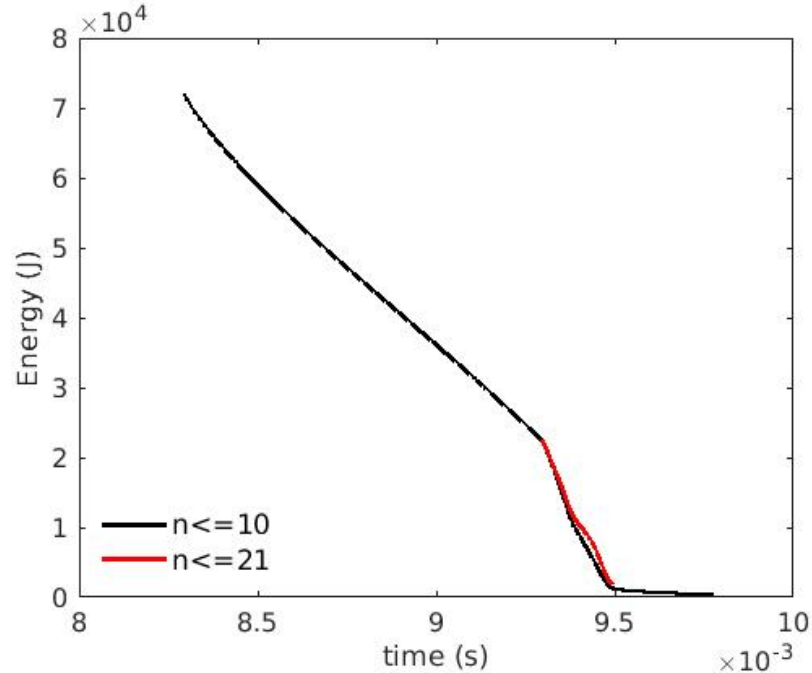
Edge pressure is lost during the initial saturation of the MHD activity.



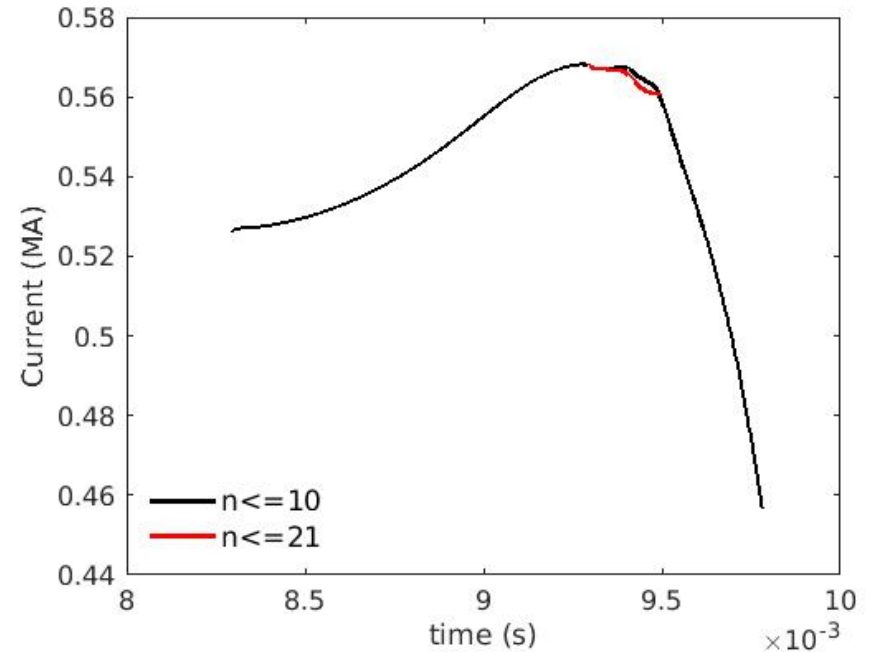
- Pressure in NIMROD's $\phi = 0$ plane of the $0 \leq n \leq 21$ computation shows rapid evolution during this initial saturation.
- The (2,1) mode remains dominant, but other modes contribute.

The thermal quench accelerates due to the MHD.

- The TQ is started by the changes in κ_{\perp} and D that are imposed at the start of the 3D computation.
- The effect on plasma current is minimal until electrical conductivity is lost.



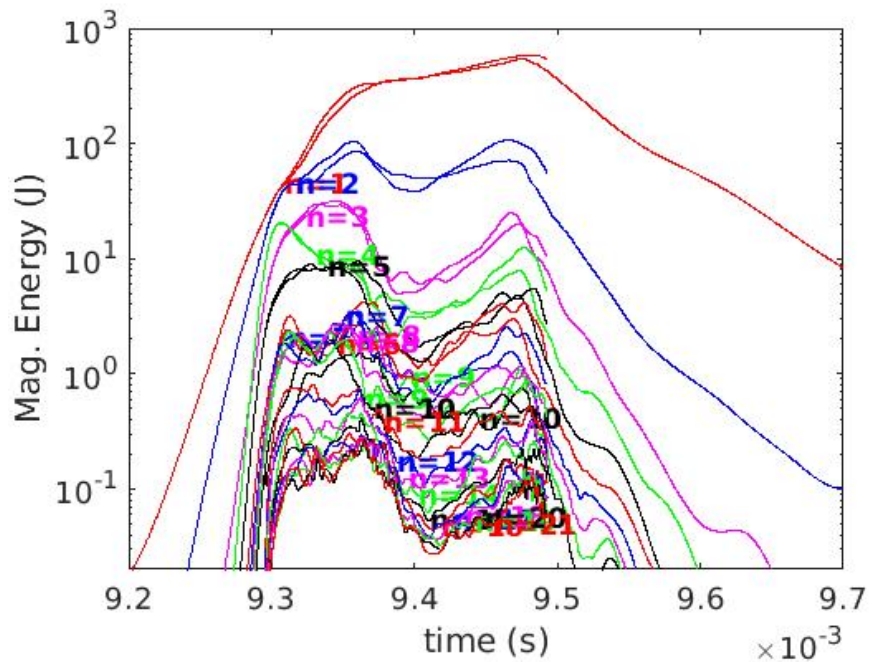
Evolution of internal energy from computations with different toroidal resolution.



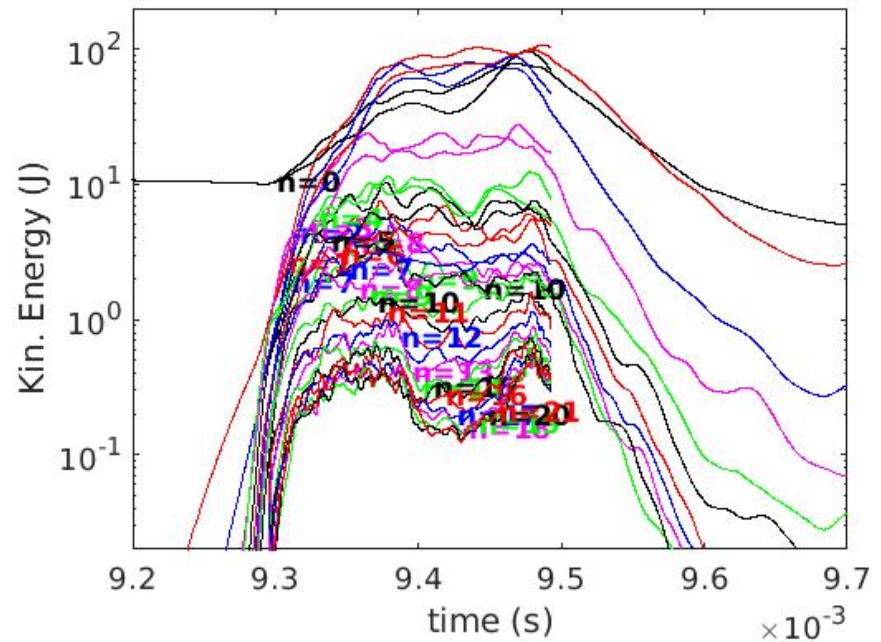
Evolution of plasma current from the two computations.

Increasing resolution from $n \leq 10$ to $n \leq 21$ has minimal impact on the dominant activity.

- The larger- n harmonics were added at 9.3 ms.
- The lower- n harmonics of the two computations track each other well.



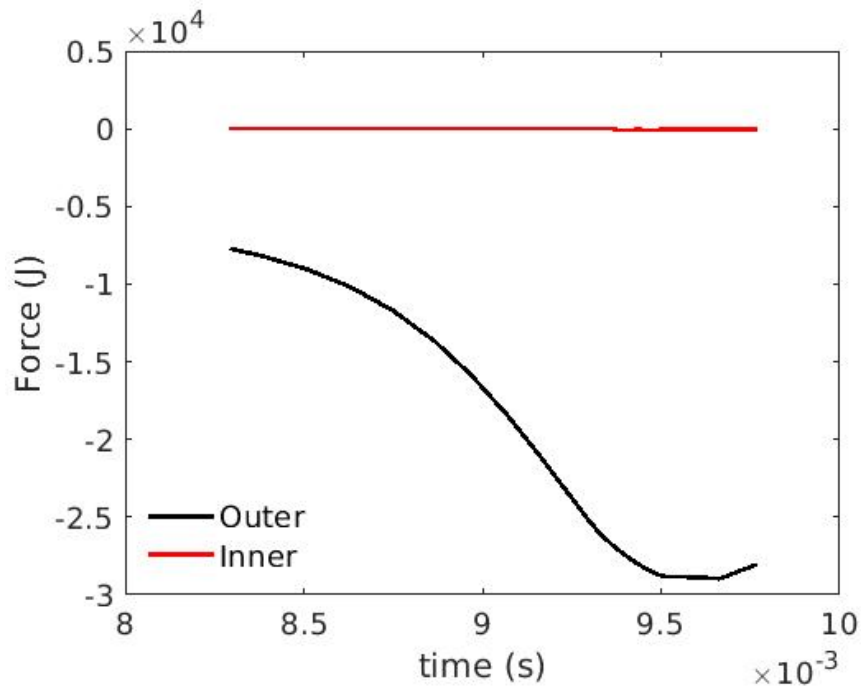
Evolution of magnetic fluctuation energies from both computations.



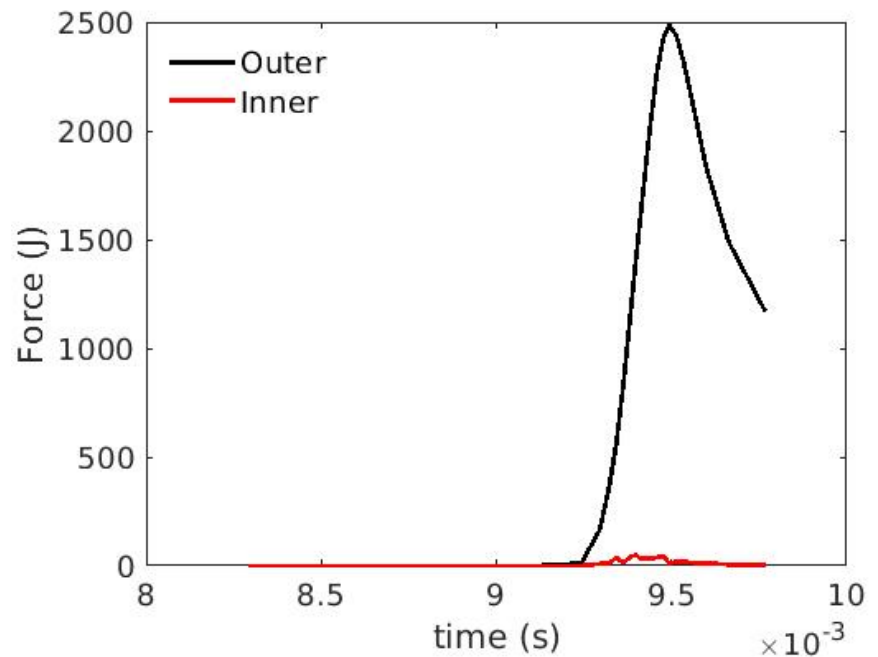
Evolution of kinetic fluctuation energies from both computations.

Integrating stress over inner and outer surfaces confirms expectations on force.

- The inner force is negligible; thus, the plasma remains in force-balance with the wall.



Evolution of the vertical component of force in the $n \leq 10$ computation.



Evolution of the magnitude of horizontal force in the $n \leq 10$ computation.

- This balance of forces in non-ideal MHD computation was also shown in an idealized case in PPCF **61**, 024003 (2019).

Extra Material

M3D-C1 and NIMROD solve full-MHD equations.

- M3D-C1 solves the equations in potential form.
- NIMROD solves them in primitive form.

$$\frac{\partial n}{\partial t} + \nabla \cdot (n\mathbf{V}) = \nabla \cdot (D\nabla n)$$

$$\rho \left(\frac{\partial}{\partial t} \mathbf{V} + \mathbf{V} \cdot \nabla \mathbf{V} \right) = \mathbf{J} \times \mathbf{B} - \nabla p - \nabla \cdot \mathbf{\Pi}$$

$$\frac{3}{2} n \left(\frac{\partial}{\partial t} T + \mathbf{V} \cdot \nabla T \right) = -\frac{p}{2} \nabla \cdot \mathbf{V} + \nabla \cdot [(\kappa_{\parallel} - \kappa_{\perp}) \hat{\mathbf{b}} \hat{\mathbf{b}} + \kappa_{\perp} \mathbf{I}] \cdot \nabla T - T \nabla \cdot (D\nabla n)$$

$$\frac{\partial}{\partial t} \mathbf{B} = \nabla \times (\mathbf{V} \times \mathbf{B} - \eta \mathbf{J})$$

- The particle-diffusivity energy **correction** was added to NIMROD during the 2D benchmarking.
- NIMROD's simplest thermal conduction typically uses constant diffusivity values and not constant conductivities.
 - A variant was developed to match M3D for benchmarking.
 - NIMROD's $\mathbf{\Pi}_{\parallel} = \nu_{\parallel} \hat{\mathbf{b}} \cdot \mathbf{W} \cdot \hat{\mathbf{b}} (\mathbf{I} - 3\hat{\mathbf{b}}\hat{\mathbf{b}})$, $\mathbf{W} = \nabla \mathbf{V} + \nabla \mathbf{V}^T - (2/3)\mathbf{I} \nabla \cdot \mathbf{V}$

JOREK is used to solve the reduced-MHD equations.

$$\frac{\partial \rho}{\partial t} + \nabla \cdot (\rho \mathbf{V}) = \nabla \cdot (D \nabla_{\perp} \rho)$$

$$\hat{\boldsymbol{\phi}} \cdot \nabla \times \left(\rho \frac{\partial}{\partial t} \mathbf{V} + \rho \mathbf{V} \cdot \nabla \mathbf{V} \right) = \hat{\boldsymbol{\phi}} \cdot \nabla \times (\mathbf{J} \times \mathbf{B} - \nabla p + \mu \nabla^2 \mathbf{V})$$

$$\mathbf{B} \cdot \left(\rho \frac{\partial}{\partial t} \mathbf{V} + \rho \mathbf{V} \cdot \nabla \mathbf{V} \right) = \mathbf{B} \cdot (\mathbf{J} \times \mathbf{B} - \nabla p + \mu \nabla^2 \mathbf{V})$$

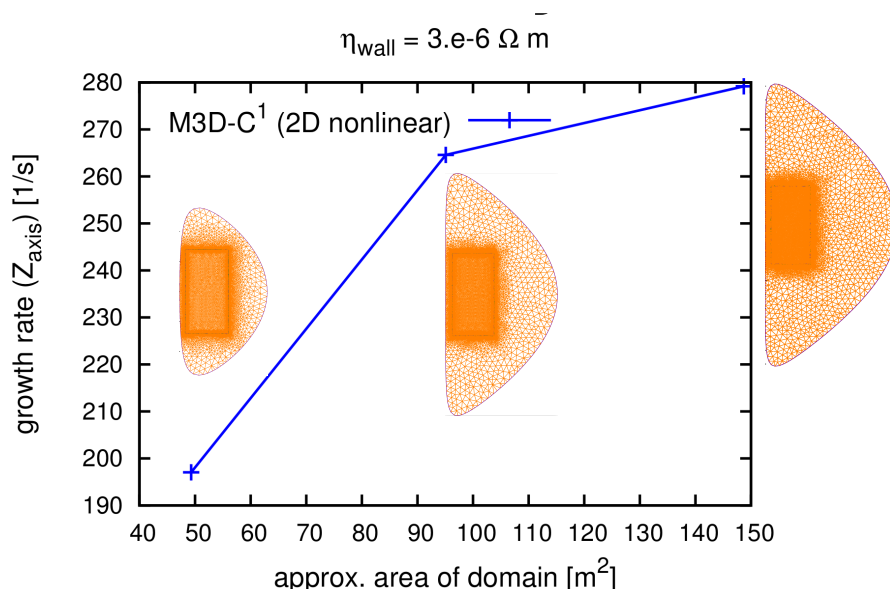
$$\frac{\partial}{\partial t} p + \mathbf{V} \cdot \nabla p = -\gamma p \nabla \cdot \mathbf{V} + (\gamma - 1) \nabla \cdot [\kappa_{\parallel} \nabla_{\parallel} + \kappa_{\perp} \nabla_{\perp}] \left(\frac{p}{\rho} \right)$$

$$\frac{1}{R^2} \frac{\partial \psi}{\partial t} = \eta \nabla \cdot \left(\frac{1}{R^2} \nabla_{\perp} \psi \right) - \mathbf{B} \cdot \nabla u$$

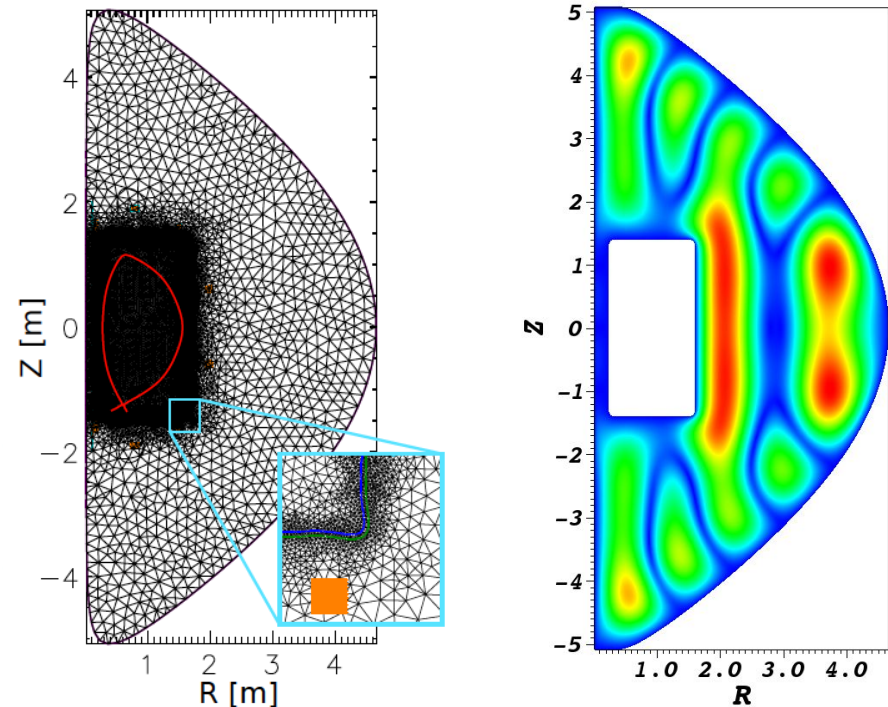
- See Huysmans, *et al.*, PPCF **51**, 124012 (2009).
- The variable u above is the streamfunction for \mathbf{V}_{\perp} .

Unlike JOREK, NIMROD and M3D-C1 use meshed numerical computations of external vacuum-field response.

- NIMROD couples inner and outer regions via the thin-wall model.
- M3D-C1 meshes across the resistive wall.
- JOREK couples to the STARWALL code (no outer conducting wall).



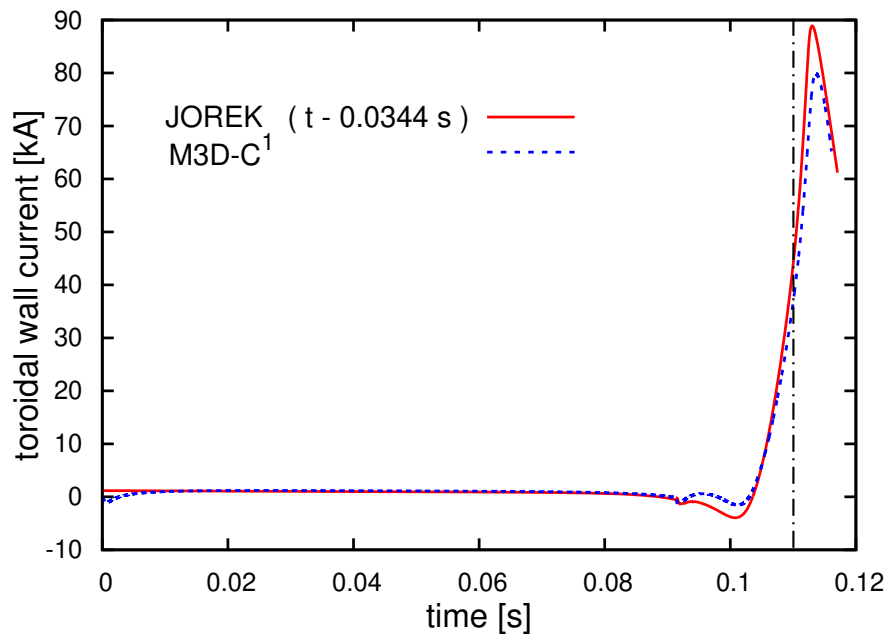
Krebs evaluated dependence on the vacuum region size.



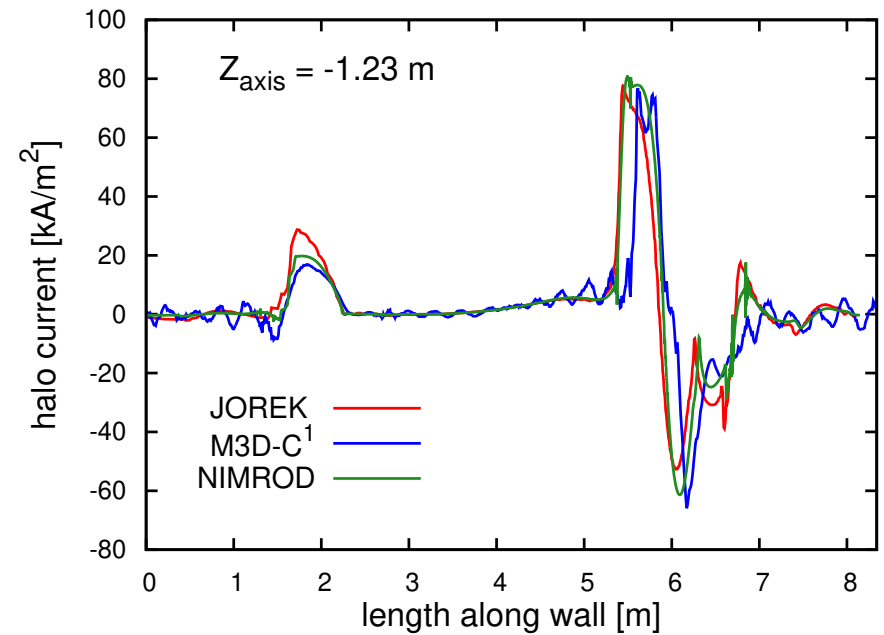
New NIMROD outer region (right – test waves plotted) is nearly the same as M3D-C1's (left).

The late-time distributions of J -normal agree reasonably well.

- The JOEREK reduced-MHD edge $\mathbf{J}_{\text{pol}} = J_{\text{tor}} \mathbf{B}_{\text{pol}} / B_{\text{tor}}$.
- Locations and magnitudes of current density concentration are consistent.

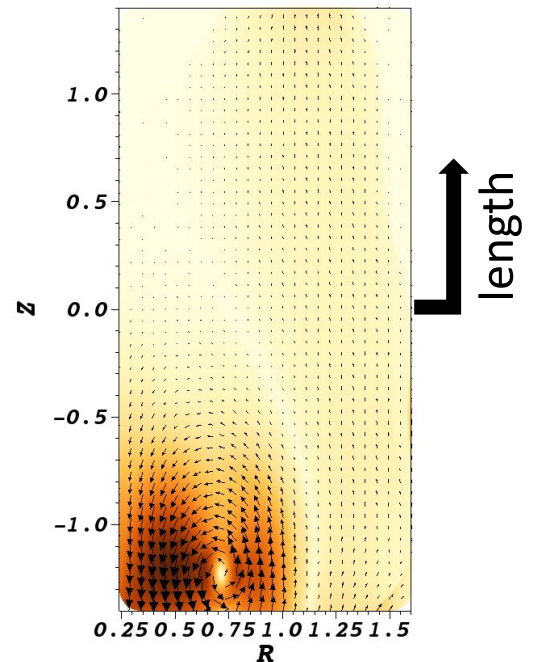


I_{wall} vs. t has been extracted for M3D-C1 and JOEREK. Vertical line is time of J -normal plot.



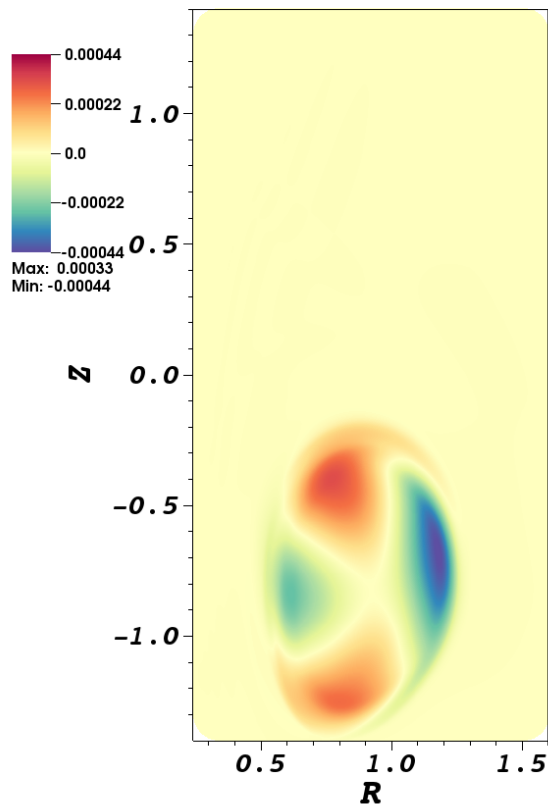
J -normal (halo) vs. position along wall, measured counter-clockwise.

Plot of J_{pol} (right) indicates where halo current enters and exits central region.

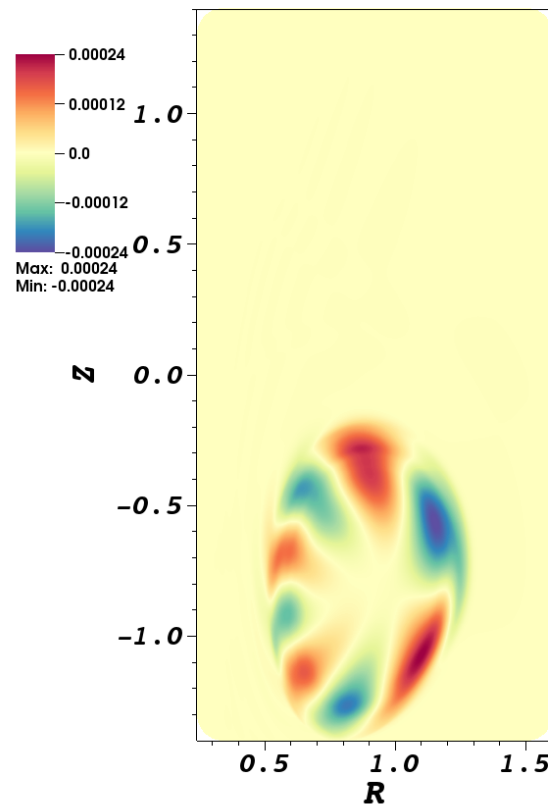


At the time of their rapid growth, the instabilities are largely harmonics of (2,1).

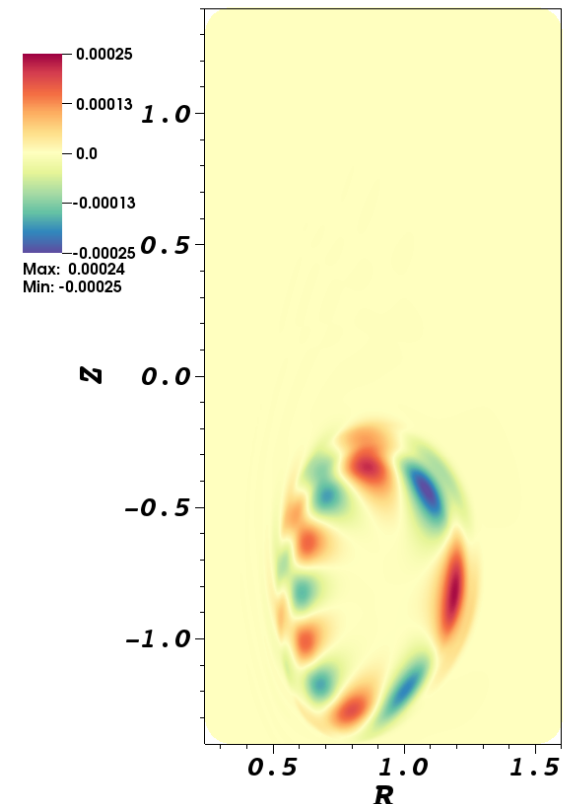
- Plots of individual toroidal Fourier components of pressure at $t = 9.3$ ms show these harmonics.
- The $n=3$ component is a mix of (5,3) and (6,3).



Contours of constant pressure for $n=1$.



Contours of constant pressure for $n=2$.



Contours of constant pressure for $n=3$.